Alzheimer's-Induced Changes in Grid Cell Electrophysiology Affect Path Integration in a Network Model of the Medial Entorhinal Cortex

A thesis
Submitted towards the partial fullfilment of
BS-MS dual degree programme
by

SRIRANG NABAR

Date: 16/03/2025

under the guidance of

DR COLLINS ASSISI

DEPARTMENT OF BIOLOGY

from May 2024 to Mar 2025

Indian Institute of Science Education and Research
Pune

Certificate

This is to certify that this dissertation entitled "Alzheimer's-Induced Changes in Grid Cell Electrophysiology Affect Path Integration in a Network Model of the Medial Entorhinal Cortex" submitted towards the partial fulfillment of the BS-MS degree at the Indian Institute of Science Education and Research, Pune represents original research carried out by Srirang Nabar at IISER Pune, under the supervision of Dr Collins Assisi during academic year 2024-2025.

Supervisor:
Dr Collins Assisi
Assistant Professor
Department of Biology

Srirang Nabar
20201185
BS-MS
IISER Pune

Date: 16/03/2025

Declaration

I, hereby declare that the matter embodied in the report titled "Alzheimer's-Induced Changes in Grid Cell Electrophysiology Affect Path Integration in a Network Model of the Medial Entorhinal Cortex" is the results of the investigations carried out by me at the Indian Institute of Science Education and Research, Pune under the supervision of Dr Collins Assisi and the same has not been submitted elsewhere for any other degree.

Supervisor:
Dr Collins Assisi
Assistant Professor
Department of Biology

Srirang Nabar
20201185
BS-MS
IISER Pune

Date: 16/03/2025

Acknowledgements

This thesis would not have been possible without the support, guidance, and encouragement of many incredible individuals, to whom I am deeply grateful.

First and foremost, I would like to express my heartfelt gratitude to my advisor Dr Collins Assisi, and the members of the Theoretical Neuroscience and Computational Neurobiology labs, whose insights, patience, and expertise have shaped this work. Their unwavering support and intellectual generosity made my research journey both challenging and rewarding. A special acknowledgment goes to Inayath Shaikh, whose work on the grid cell model has been instrumental. His research laid the foundation for this study, and his contributions and patient mentorship have greatly influenced my approach.

I am also grateful to my sponsors, whose funding and resources enabled me to pursue this research—your belief in my potential has been invaluable. Because of this support, I had access to the tools and training that allowed me to explore fascinating and important questions at the frontiers of scientific knowledge. In particular, I would like to thank the KVPY Fellowship, the IDeaS Pune Scholarship, and the CNR Rao Education Foundation for their generous contributions, which made my education at IISER Pune possible.

My deepest thanks go to my family - Aai, Baba and Anu, whose love has been the roots that have kept me grounded and the wind that has helped me soar. Your strength, sacrifices, and endless encouragement have shaped who I am today. This achievement is as much yours as it is mine.

To my friends and mentors who have been there through the highs and lows, offering words of encouragement, laughter, and support — thank you for keeping me grounded and reminding me of the joy in the journey. Everytime I faltered, I had your support to lean on, and your belief in me has been a constant source of strength. Thank you giving me the courage to pursue my dreams.

This thesis is a testament to all of you. We are each a patchwork quilt of those who have loved us, taught us, and inspired us. I am grateful for the threads you have woven into my life.

Contributions

Contributor name	Contributor role
Dr Collins A. and Srirang N.	Conceptualization Ideas
Inayath S. and Srirang N.	Methodology
Inayath S. and Srirang N.	Software
Srirang N.	Validation
Srirang N.	Formal analysis
Srirang N.	Investigation
Dr Collins A., Inayath S. and Srirang N.	Resources
Srirang N.	Data Curation
Srirang N.	Writing - original draft preparation
Dr Collins A. and Srirang N.	Writing - review and editing
Srirang N.	Visualization
Dr Collins A.	Supervision
Dr Collins A. and Srirang N.	Project administration
Dr Collins A.	Funding acquisition

This contributor syntax is based on the Journal of Cell Science CRediT Taxonomy[1]

[1]https://journals.biologists.com/jcs/pages/author-contributions

Abstract

Alzheimer's disease (AD) is the leading cause of dementia in the modern day, due to the rapid increase in life expectancy across the developed world. While there is no known cure for AD, a sufficiently early diagnosis can precipitate better outcomes in terms of preserving the quality of life experienced by AD patients. In the earliest stages of AD, studies have reported abnormalities in the electrophysiological properties of neurons in the entorhinal cortex (EC), a region of the brain that plays a crucial role in spatial navigation. In particular, grid cells in the EC have been shown to exhibit altered firing patterns in AD patients. Grid cells are neurons that fire in a spatially periodic manner, and are thought to be responsible for the brain's ability to form cognitive maps of the environment. Using a biophysically-realistic computational model of the grid cells, we have investigated the effects of varying electrophysiological properties in the EC on the network dynamics of grid cells. Our results show that altering certain electrophysiological properties lead to changes in the spatial periodicity of the grid cells, creating a signature which could potentially be used as a diagnostic tool for AD. While further work is needed to validate these results, our study provides a proof-of-concept for the use of computational models in understanding the pathophysiology of AD.

Contents

Chapter 1

Introduction

As a result of the blistering pace of advancement in the medical sciences, the average life expectancy in the developed world has skyrocketed by nearly 30 years in the last century, precipitating the rise of senescence-related ailments like Alzheimer's disease (AD) (Boudoulas *et al.* (2017)). Thus, the need for a deeper understanding of the mechanisms underlying AD has never been more pressing. This chapter will provide an overview of the "required reading" necessary to understand the context of this study - including a brief report on AD and its progression, grid cells, and the link between the entorhinal cortex and AD. In this study, we aim to investigate the effect of AD-like conditions on grid cells in the entorhinal cortex of using a computational model described in Chapter 2.

1.1 Background

Spatial memory and navigation have been topics of considerable interest in the field of neuroscience ever since Tollman's seminal experiments in the 1940s prompted him to postulate the existence of a "cognitive map" in the brain that could store spatial information, as well as mechanisms to learn, update and retrieve this information (Tolman (1948); Bellmund *et al.* (2018)). Over two decades later, a neural basis for such a cognitive map was discovered in the hippocampus when O'Keefe and Dostrovsky (1971) found that rats with hippocampal damage performed poorly on spatial tasks. Further experiments discovered spatially-selective pyramidal neurons dubbed place cells which fire when the animal is in a specific location in the environment (O'Keefe (1976); O'Keefe and Nadel (1978)), providing substantial evidence for the existence of the theorized cognitive map.

While such a map is essential for executing spatial tasks, it is not suffi-

cient. A static map in the hippocampus would not be able to account for the process of hippocampal remapping, a process by which place cells rapidly change their firing fields when the animal is placed in a novel environment (O'Keefe and Burgess (1996)). This suggests that the hippocampal cognitive map is not static, but rather there must exist upstream computational mechanisms that continually relay information about the environment to the hippocampus. For example, a representation of directionality was discovered by Taube *et al.* (1990) in the form of head direction cells in the postsubiculum, which fire when the animal faces a specific direction in the environment.

It is known that the entorhinal cortex (EC) is a major source of inputs to the hippocampus, and these projections are arranged in a precise topological pattern, with bands of entorhinal neurons projecting to specific regions of the hippocampus. This led to the hypothesis that the EC might host a neural mechanism that could serve as a consistent measure of spatial distances (O'Keefe and Nadel (1978)).

1.2 Grid Cells

Located in the medial entorhinal cortex (MEC), grid cells are neurons with egocentric hexagonally/triangularly tessellating firing fields as seen in Figure 1.1 B. First described by Hafting *et al.* (2005), grid cells are thought to provide a metric for spatial distances as well as a representation of directionality. The discovery of grid cells was a major breakthrough in the field of cognitive neuroscience. May-Britt Moser and Edvard I. Moser, along with John O'Keefe, were awarded the Nobel Prize in Physiology or Medicine in 2014 for their insights into how our brains represent the world around us (Burgess (2014)).

Grid cells remain an active area of research; Moreover, the importance of other network mechanisms is also being explored. For example, Schlesiger *et al.* (2018) discovered that global remapping in the hippocampus is not solely dependent on MEC inputs. Similarly, the exact mechanisms by which grid cells generate their firing patterns are still not fully understood, though several credible models have been proposed (Burgess and O'Keefe (2011); Giocomo *et al.* (2011)). We will discuss our model in greater detail in Chapter 2.

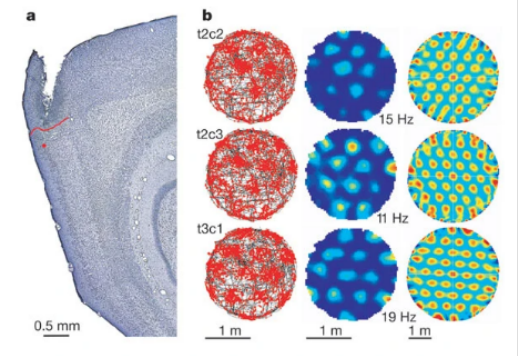

Figure 1.1: **A**: The medial entorhinal cortex, highlighted in red is the track along which the corresponding recordings were obtained. **B**: Firing fields of three grid cells. Left column - trajectory of the rat (black) with locations where the cell spiked superimposed (red). Middle column - firing rate map, with maximum record rate. Blue is low, red is high. Right column - Spatial autocorrelation for the rate map. Adapted from Hafting *et al.* (2005).

1.3 Alzheimer's Disease

Alzheimer's disease (AD) is a progressive neurodegenerative disease characterised by protein agglomerates, neurofibrillary tangles and an accumulation of amyloid and tau proteins in neurons and cerebrospinal fluid (Yaari *et al.* (2011)), and it is a leading cause of dementia (Reitz *et al.* (2011)). Although studies project that by 2050 approximately 100 million patients will suffer from AD, currently available treatments only provide symptomatic relief and do not address the underlying causes of the disease (Breijyeh and Karaman (2020); Galimberti and Scarpini (2011)).

The dominant model of AD pathogenesis is the amyloid cascade hypothesis, which posits that the accumulation of insoluble amyloid-β peptides (the proteolytic product of the larger Amyloid Precursor Protein, also known as APP) in the brain is the primary cause of the disease (Hardy and Higgins (1992)). Though the instigating causes of this amyloid build-up are still unknown (and likely multifactorial and intercorrelated), some risk factors are known. For example, according to Liu *et al.* (2013), human carriers of the $\varepsilon 4$ allele of Apolipoprotein E (APoE) have a higher-risk of developing AD later in life. This makes sense, as APoE is known to bind amyloid-β peptides and prevent the build-up of toxic aggregates. In fact, given the failures of amyloid-targeting drugs in clinical trials, it is likely that the characteristic amyloid plaques are downstream symptoms of the disease, rather than the

root cause.

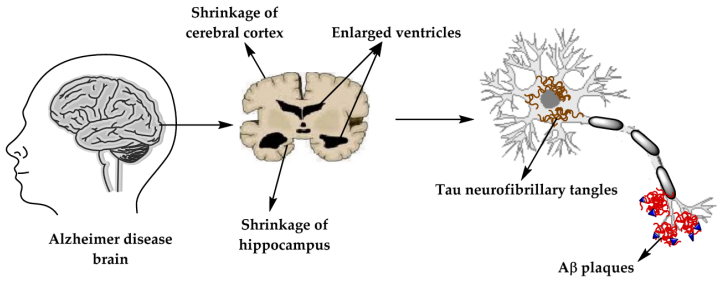

Figure 1.2: Typical characteristics of Alzheimer's disease across scales (Breijyeh and Karaman (2020)).

The initial progression of AD is characterised by a prodromal or preclinical stage where cellular and molecular damage accumulates in the brain without any noticeable cognitive symptoms for over a decade, (Bateman *et al.* (2012); Buchhave *et al.* (2012); Funato *et al.* (1998)). It is important to note that this stage (Braak stages I and II) is only "invisible" to external observers; the brain is already undergoing significant and measurable changes - according to Fagan *et al.* (2014) the cerebrospinal fluid (CSF) levels of biomarkers of AD pathology are altered (amyloid-β_{1-42} concentrations are reduced, while tau and phosphorylated tau concentrations are increased), and according to Dubois *et al.* (2016) evidence for brain amyloidosis can be detected using positron emission tomography (PET) imaging.

Next, the disease progresses to a mild cognitive impairment (MCI) stage, where the patient experiences moderate memory deficits (missing appointments, forgetting items, etc.) noticeable to the patient and their family, but not severe enough to meet reasonable diagnostic criteria for dementia (Petersen *et al.* (1999)). It is in this stage (also designated as Braak stages III and IV) that hippocampal dysfunction is observed in animal models of AD (Jun *et al.* (2020)). It should be noted, however, that transgenic animal models of AD are poor representations of human AD and its progression, as characterised by the drastic differences in the onset and progression of defects and abnormalities in various transgenic models (see Figure 1.3). This is likely due to the fact that these animals develop AD due to an artificial overexpression of human genes, and not due to the natural progression of the disease. Thus, while the insights gained from experiments conducted on these models is valuable, we should take care when extrapolating these results to the progression of the disease in human patients, as no currently available mouse model accurately mimics the accumulation of amyloid-β and tau proteins in

the human brain in most cases of AD (Yokoyama *et al.* (2022)).

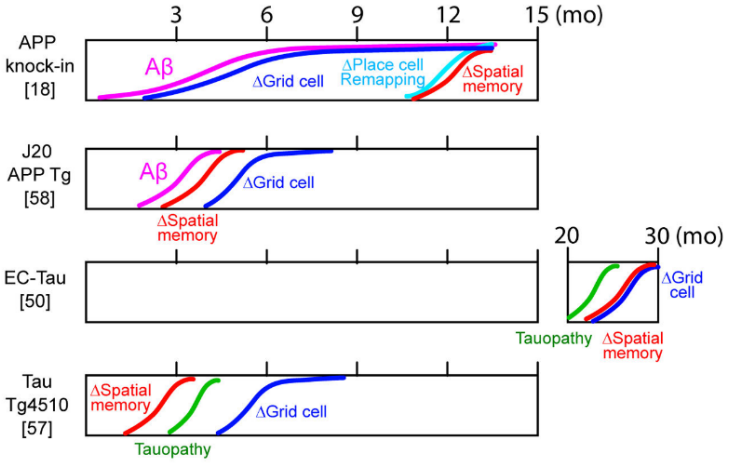

Figure 1.3: Schematic summary of differences in the progression and onset of defects and abnormalities associated with AD in various transgenic mouse lines. Figure taken from Igarashi (2023).

The final stage of AD is characterised by severe cognitive impairment and dementia, with the patient experiencing severe memory loss, disorientation, and difficulty in performing daily tasks. This is usually the point where a patient is diagnosed with dementia. Even at the very beginning of this stage, widespread irreversible neurodegeneration has ravaged the brain (see Figure 1.2). Gómez-Isla *et al.* (1996) showed that layer II of the EC (where grid cells are located) in patients with even the mildest clinically detectable dementia had a 32% fewer neurons than similarly-aged cognitively-normal individuals. This figure can rise to 90% as the disease progresses. A similar depletion of neurons in the EC is observed in animal models of AD as well (Chin *et al.* (2007)).

1.3.1 Preclinical Alzheimer's Disease

As described in §1.3 and shown in Figure 1.5 B, by the time a patient is typically diagnosed with AD, significant neurodegeneration has already occurred. It is unlikely that any medical interventions would able to reverse the damage done to the brain at this stage and restore cognitive functions. However, if the disease is caught early before it has the chance to cause widespread cell death, it is feasible that once the mechanisms behind the causes of AD are better understood, a cure that could halt or reverse the molecular damage

caused by the disease could be developed. Thus, an early diagnosis of AD (perhaps via the implementation of a age-based screening procedure as part of routine outpatient medical check-ups) combined with a better understanding of the causes facilitating the failures in the molecular machinery could help develop treatments that may preserve cognitive functions and lead to better patient outcomes in the next few decades (Igarashi (2023); Sperling *et al.* (2011)).

As discussed above in §1.3, evidence for the pathophysiology of AD is detectable in CSF samples and PET scans in the preclinical stage. However, testing the CSF via lumbar puncture is invasive, and PET scans are expensive and risk radiological exposure (Schöder and Gönen (2007)). Neither of these methods are suitable for routine screening of patients at risk of developing AD. Thus, there is a need for a non-invasive, cost-effective, and easily accessible method for early diagnosis of AD. Given the involvement of the EC in the early stages of AD, screening for defects in spatial-information processing functions controlled by the EC could be early non-invasive and low-risk methods for diagnosing preclinical AD.

One potential pathway for diagnostic research might come from research done by Bierbrauer *et al.* (2020), who found that APoE-ε4 carriers with normal cognitive abilities show reduced path integration performance in a virtual navigation task compared to a non-carrier control group when no boundary or landmark cues are present (See Figure 1.4). The presence of this defect in "pure" path integration and the absence of noticeable defects in assisted path integration points to two conclusions: First, there may be compensatory mechanisms that support the path integration process when given spatial cues, like boundary cells and object-vector cells (Solstad *et al.* (2008); Høydal *et al.* (2019)). Second, understanding the ways grid cells behave differentially in AD could provide a mechanistic understanding of preclinical AD progression; Bierbrauer *et al.* (2020) propose that the path integration deficits are caused by grid cell dysfunction, based on the fMRI study correlating poor grid-like representations in the EC with poor navigational performance. Thus, understanding the effects of AD-like conditions on grid cells in the EC could be useful in understanding these defects and support the creation of new diagnostic techniques.

1.3.2 Grid Cells in Alzheimer's Disease

The entorhinal cortex is one of the first regions to be affected by AD, and it is also where the first signs of dysfunction are observed (see second row of Figure 1.5 B) (Igarashi (2023)).

Many studies have explored the differential behaviour of grid cells in AD

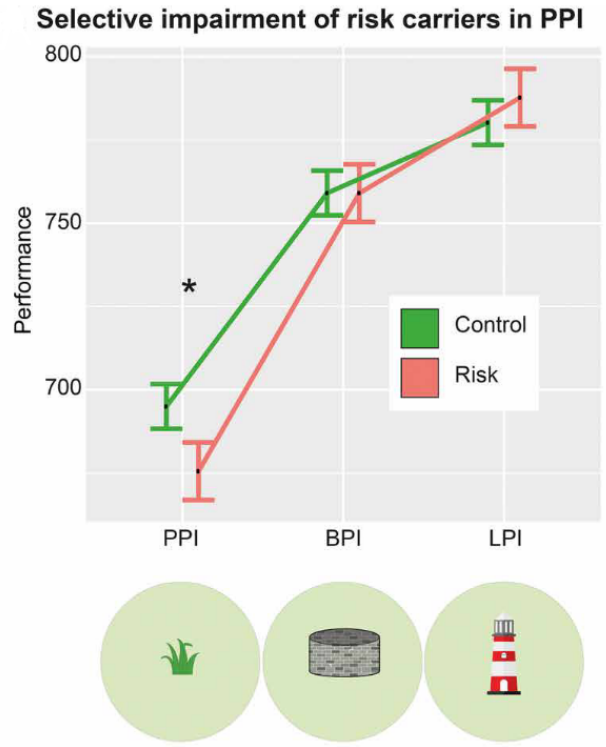

Figure 1.4: The path integration performance of APoE-ε4 carriers and non-carriers in the virtual navigation task. Here PPI stands for "pure" path integration, while BPI and LPI stand for boundary-assisted and landmark-assisted path integration respectively. Figure taken from Bierbrauer *et al.* (2020).

models. While studying place cell remapping in an APP knock-in (APP KI) mouse model of AD, Jun *et al.* (2020) found that young (3 to 5 months old) APP KI mice had similar spatial memory performance as young wildtype (WT) mice despite the presence of amyloid-β plaques in the hippocampus and the MEC, but old (7 to 13 months old) APP KI mice perform significantly worse than old WT mice in Y-maze tasks and discriminating between two distinct environmental context. The authors propose that this due to the differential place cell remapping ability in young and old APP KI mice. However, the study also discovered that MEC dysfunction emerges early, and is already present in young APP KI mice. Electrophysiological recordings found that EC cells showed lower spatial selectivity in young APP KI mice compared to young WT mice, which provides more mechanistic evidence for the results of Bierbrauer *et al.* (2020) as discussed above.

What are the mechanisms involved in the dysfunction of grid cells in AD models? We can gain some insights from single-cell electrophysiological studies that have been conducted in AD model systems. Heggland *et al.* (2019) found increased excitability in stellate cells of McGill-R-Thy1-APP transgenic rats. Specifically, they demonstrated that the stellate cells had an increased initial frequency of firing in response to injected current, which the authors attributed to altered calcium-dependent potassium (K_{Ca}) channels (see Figure 1.6 A). The results of Marcantoni *et al.* (2014) reinforce the existence of such hyperexcitability, as they showed a reduced interspike interval (ISI), that is, the time between two successive action potentials in grid cells of Tg2576 mice, as seen in Figure 1.6 B.

From electrophysiological studies like the ones mentioned above, as well as from single-channel studies, it is clear that the dysfunction of grid cells in AD is, in part, likely due to changes in the electrophysiological properties of K_{Ca} channels (Trombetta-Lima *et al.* (2020)). For instance, it is known that amyloid-β peptides can bind Homer1a, which results in the suppression of large conductance K_{Ca} (BK) channels in 3xTg AD model mice, and deficits in spatial memory performance in these mice are ameliorated by isopimaric acid, a BK channel opener (Yamamoto *et al.* (2011); Wang *et al.* (2015)). Thus, to investigate the effects of AD-like conditions on grid cells in the EC, we need to mimic this K_{Ca} channel dysfunction and replicate the results of Heggland *et al.* (2019) and Marcantoni *et al.* (2014) in our computational model.

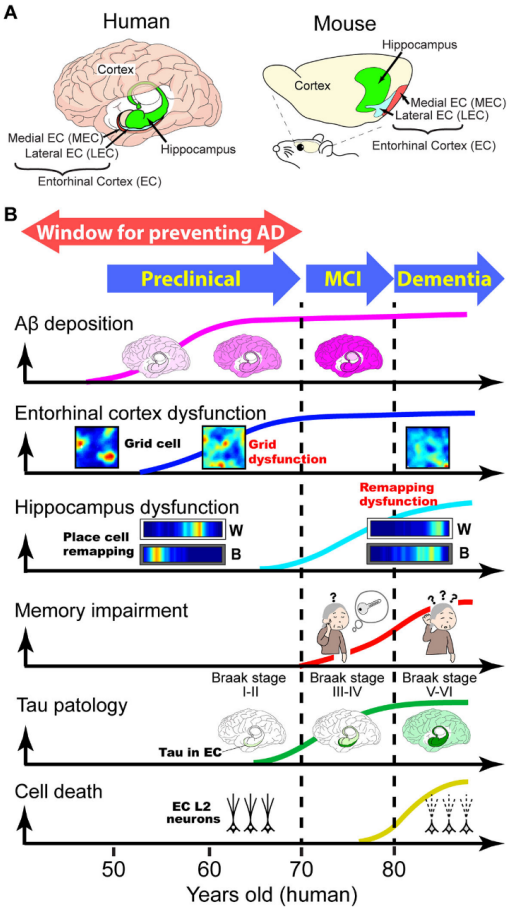

Figure 1.5: **A**: A diagram showing the EC and hippocampus in humans and mice, two regions heavily involved in episodic memory, spatial navigation and Alzheimer's disease progression. **B**: A heuristic diagram depicting the putative time course of the progression of Alzheimer's disease in human and animal models. Figure taken from Igarashi (2023).

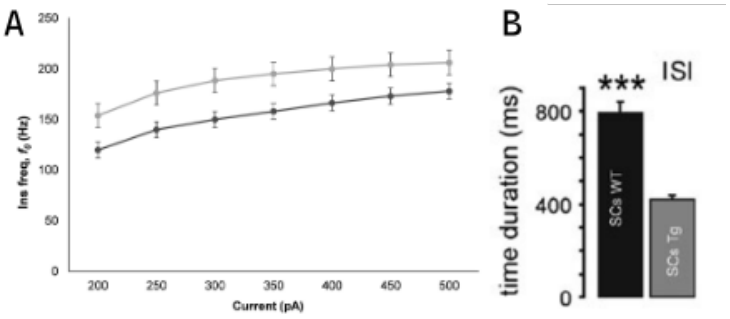

Figure 1.6: **A**: The initial firing rate of stellate cells in wildtype and McGill-R-Thy1-APP transgenic rats as a function of the strength of depolarizing current. Figure taken from Heggland *et al.* (2019). **B**: The interspike interval (ISI) of grid cells in wildtype and Tg2576 mice. Figure taken from Marcantoni *et al.* (2014). In both cases, light grey depicts the AD model group, and dark grey depicts the wildtype control group.

Chapter 2

Model

To investigate the effects of varying electrophysiological properties in the entorhinal cortex, we have built a network model of conductance-based neurons. This model is heavily based on previous work done by the Assisi lab (Neru and Assisi (2021)), which we have extended to include a more detailed description of the calcium dynamics using simplified models of calcium currents (I_{Ca}), after-hyperpolarization currents (I_{AHP}) and calcium regulation dynamics adapted from models described in Bazhenov *et al.* (2001). The model consists of two types of neurons, Stellate cells (SC) and inhibitory Interneurons (IN), which are connected in a manner described in more detail in section 2.2. The model is driven by external inputs that carry velocity inputs, which are described in section 2.3.

2.1 Conductance-Based Models

The first conductance-based models were developed in the 1950s and 1960s by Hodgkin and Huxley (1952) based their work on the squid giant axon. They described the dynamics of the membrane potential as the voltage difference across two points, one inside and the other outside the cell, bridged by a circuit of a capacitor and conductances connected in parallel (See Figure 2.1). The capacitor emulates the membrane capacitance of the cell, and the conductances represent the ionic currents flowing across the membrane - sodium channels (g_{Na}), potassium channels (g_K), and a leak current (g_L). Thus, the membrane potential can be calculated using Kirchoff's laws, which gives us the following equation:

$$C_m \frac{dV}{dt} = I_{ext} - I_{Na} - I_K - I_L \tag{2.1}$$

These models are more computationally-expensive compared to simpler

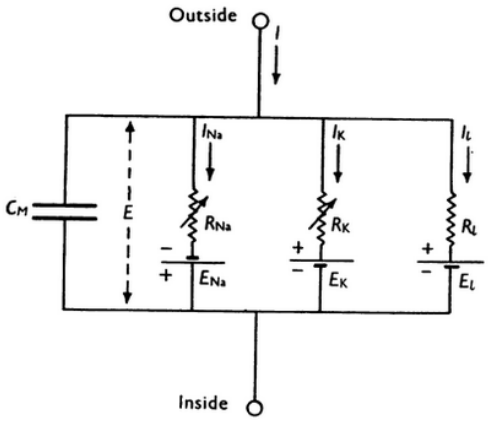

Figure 2.1: The equivalent circuit for the simplest conductance-based model of an excitable cell, the Hodgkin-Huxley model (Hodgkin and Huxley (1952)). The model consists of a membrane capacitance C_m in parallel with three conductances: sodium (g_{Na}), potassium (g_K), and leak (g_L).

models like the integrate-and-fire model, which can make them slower to simulate. However, conductance-based models are more biophysically realistic than these simpler models, as they allow us to explicitly and independently model various ionic channels and mechanisms. This makes the model more tractable, as it allows us to investigate the effects of varying electrophysiological properties on network dynamics, which is not possible with simpler models.

Our model is more complex than the Hodgkin-Huxley model described in Equation 2.1, and is described in the following sections.

2.1.1 Basic Ion Channels and Dynamics

To model the currents flowing across the membrane we use the following equations. Any given current I_i can be defined as

$$I_i = g_i(V - E_i)$$

where g_i is the conductance of the channel, V is the membrane potential, and E_i is the reversal potential of the channel. For an ion channel, the reversal potential is calculated via the Nernst equation. Here, g_i is not a constant; it is a time-dependent variable, and is in general given by the following equation:

$$g_i = \bar{g}_i m^a h^b$$

where the constant $\bar{g}_i$ is the maximum conductance of the channel, m and h are the activation and inactivation gating variables. For example, the sodium current I_{Na} is given by the following equation:

$$I_{Na} = \bar{g}_{Na} m^3 h (V - E_{Na})$$

The dynamics of these gating variables are given by the following differential equations:

$$\frac{dm}{dt} = \alpha_m (1 - m) - \beta_m m$$
$$\frac{dh}{dt} = \alpha_h (1 - h) - \beta_h h$$

where α_m, β_m, α_h, and β_h are voltage-dependent functions.

Voltage-Gated Calcium Channels

While several studies have shown the diversity of the calcium channels present in the EC (Topczewska *et al.* (2019)), for the sake of simplicity and computational efficiency, we have found it sufficient to model a abstracted calcium current (I_{Ca}). We have done so with the following equation taken from Bazhenov *et al.* (2001).

$$I_{Ca} = \bar{g}_{Ca} m^2 h (V - E_{Ca})$$

where all the variables have the same meanings as described in §2.1.1.

Calcium-Activated Potassium (K_{Ca}) Channels

These K_{Ca} channels give rise to the after-hyperpolarization current (I_{AHP}), which is a slow, calcium-dependent potassium current. During the course of this study, we experimented with several models of after-hyperpolarization currents to find a suitable simple model. We had initially implemented the 10-state Markov model BKCa (large conductance) channel as described in Cox *et al.* (1997) and Cox (2014), but found it to be too computationally expensive for our purposes. We also simultaneously implemented multiple K_{Ca} channel models (described in Poirazi *et al.* (2003)) with varying conductances and kinetic timescales , based on the findings of Khawaja *et al.* (2007) who proved that multiple K_{Ca} currents exist within EC layer II SCs. However, we found that the simpler model described by Bazhenov *et al.* (2001) was sufficient for our purposes.

$$I_{AHP} = \bar{g}_{K_{Ca}} m(V - E_K)$$

where m is the gating variable governed by the following equation:

$$\frac{dm}{dt} = \frac{(m_\infty - m)}{\tau_m}$$

where m_∞ and τ_m are the steady-state activation and timescale of the gating variable m. Both are dependent on the intracellular calcium concentration $[Ca^{2+}]_i$ in mM.

$$m_\infty = \frac{[Ca^{2+}]_i}{([Ca_i^{2+}] + 0.02)}$$
$$\tau_m = \frac{5}{([Ca^{2+}]_i + 0.02)} \text{ (ms)}$$

Calcium Dynamics near the Plasma Membrane

This mechanism simulates the dynamics of the intracellular calcium concentration $[Ca^{2+}]_i$ in a thin shell near the plasma membrane with a thickness set by the variable "*depth*". It is adapted from Mittal and Narayanan (2018) and Poirazi *et al.* (2003). The dynamics of $[Ca^{2+}]_i$ are given by the following equation:

$$\frac{d[Ca^{2+}]_i}{dt} = \text{drive}_{Ca} + \frac{([Ca^{2+}]_\infty - [Ca^{2+}]_i)}{\tau_{Ca}}$$

where $[Ca^{2+}]_\infty$ is the steady-state calcium concentration, and τ_{Ca} is the timescale of calcium decay. "drive$_{Ca}$" is the calcium influx due to the calcium current I_{Ca}. By convention, inward current of a positive ion is considered negative, so "drive$_{Ca}$" is defined as:

$$\text{drive}_{Ca} = \begin{cases} \frac{-10000 \cdot I_{Ca}}{36 \cdot F \cdot depth} & \text{if } I_{Ca} \leq 0 \\ 0 & \text{otherwise} \end{cases}$$

2.1.2 Stellate Cells

The SCs are Reelin-expressing excitatory principal neurons found in layer II of the EC (Pérez-García *et al.* (2001)) which are modelled using the following equation:

$$C_m \frac{dV}{dt} = I_{ext_s} - I_{Na} - I_K - I_L - I_h - I_{NaP} - I_{Ca} - I_{AHP} - I_{syn} - I_{Noise} \quad (2.2)$$

where I_{ext_s} is the external current input to the cell, I_h is the hyperpolarization activated cation current, I_{NaP} is the persistent sodium current (described in detail in Neru and Assisi (2021), we have skipped it here as it is not central to our study's objectives), I_{Ca} is the calcium current, I_{AHP} is the after-hyperpolarization current, I_{syn} is the synaptic current, and I_{Noise} is a gaussian noise input.

2.1.3 Inhibitory Interneurons

The INs are modelled using the following equation:

$$C_m \frac{dV}{dt} = I_{ext_i} + I_{pulse} - I_{Na} - I_K - I_L - I_{syn} - I_{Noise} - I_\theta \quad (2.3)$$

where I_{ext_i} is the external current input to the INs, I_{pulse} is the pulse input, I_θ is the theta rhythmic current that generates subthreshold oscillations in membrane potential. I_{pulse} and I_θ are described in more detail in §2.3.

2.2 Connecting Neurons

2.2.1 Synapses

When a presynaptic neuron crosses a preset threshold voltage, we record an action potential and inject a weighted synaptic current into the post-synaptic neurons after a delay of 1 ms. The synapses are modelled similarly to the other conductances, but with a few differences in the differential equation regulating the gating variable s. The equation for the synaptic current is:

$$I_{syn} = W \bar{g}_{syn} s (V_{post} - E_{syn})$$

where I_{syn} is the current injected into the post-synaptic cell, V_{post} is the membrane potential of the post-synaptic cell, W is the weight (representing the strength of the synaptic connection), and E_{syn} is the reversal potential of the synapse. The reversal potential determines whether the synapse is excitatory when set to 0 mV or inhibitory when set to -80 mV. The dynamics of the gating variable s are given by the following equation:

$$\frac{ds}{dt} = F(V_{pre})\alpha_s(1-s) - \beta_s s$$

where $F(V_{pre}) = \frac{1}{2}(1 + \tanh(\frac{V_{pre}}{4}))$ is the presynaptic voltage-dependent function that models the opening of the synapse-associated ion channels.

2.2.2 The Motif

The basic connectivity motif in our model is depicted in Figure 2.2. The SCs don't interact with each other directly, but they do provide excitatory inputs to the IN directly opposite them. The INs inhibit each other, while also inhibiting the SC diagonally opposite them. This kind of inhibitory network architecture has been proposed to exist throughout the EC (Couey *et al.* (2013); Nilssen *et al.* (2018)) to explain the tight and sequential burst firing patterns of principal neurons. The interneurons are set to fire continuously, but due to reciprocal inhibition, only one fires. Here, SCs fire when subjected to hyperpolarizing inputs due to (I_h). This drive allows a SC to fire and switch which IN is firing, giving us rhythmic switching behaviour which is the basis for the phase-shifted grid fields observed in the EC.

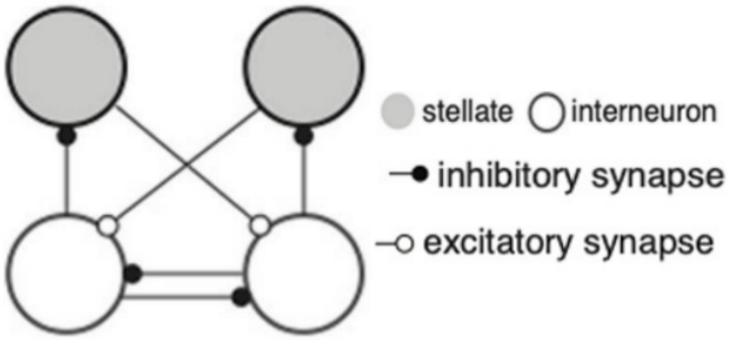

Figure 2.2: The motif model proposed by Neru and Assisi (2021)

2.2.3 Connectivity Kernel and Ring Model

The final model is a ring network of 303 neurons, with a ring of 101 INs sandwiched between two rings of 101 SCs each. The connectivity strengths between the SCs and INs is modelled with Gaussian kernels, as seen in the right half of Figure 2.3. As seen in the figure, the INs provide symmetric inhibitory inputs to both SC rings, while the SC rings provide asymmetric

excitatory inputs to the IN ring. One of the SC rings has a connectivity kernel that is biased towards the "right" or "clockwise" direction, while the other is biased towards the "left" or "counter-clockwise" direction.

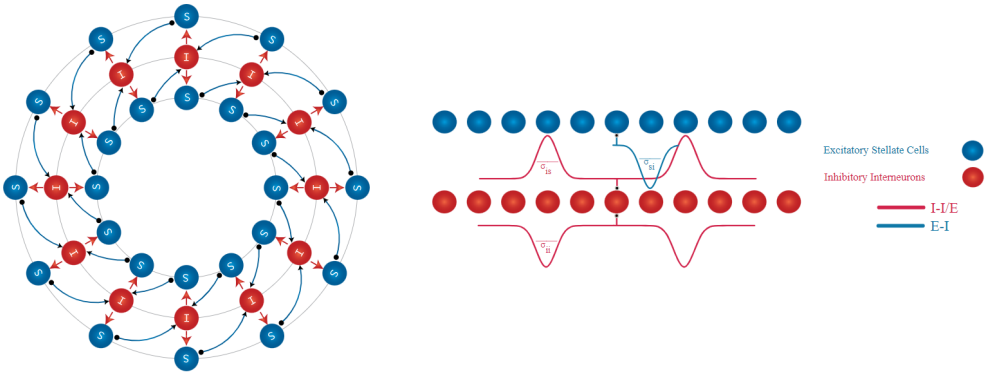

Figure 2.3: The pattern of connectivity between Stellate cells and Interneurons in the model. Figure made by Inayath Shaikh.

One of the SC rings is driven by a constant external current input I_{ext_s}, while the other is kept silent. Since the SCs can only provide "positive" inputs to the INs, two rings are needed to convey the direction of movement: The active ring determines the direction of movement, and the strength of the drive provided to it encodes the speed of movement.

2.3 External Inputs

These external inputs in our model are the same as those from the model proposed by Neru and Assisi (2021). The SCs and INs are both given constant external current inputs I_{ext_s} and I_{ext_i}, respectively. Our simulations only deal with constant velocity inputs, and thus in this case I_{ext_s} encodes velocity information as mentioned in §2.2.3.

The interneurons are given rhythmic theta inputs, modelled as sinusoidal inputs with an amplitude A, threshold voltage V_{th} and a frequency ω. The current injected into the interneurons is given by the following equation:

$$I_\theta = A\sin(2\pi\omega t + \phi)(V - V_{th})$$

Chapter 3

Methods

As mentioned in Chapter 2, to investigate the effects of varying electrophysiological properties in the entorhinal cortex, we simulated a network model of single-component conductance-based neurons. This chapter describes the particulars of the these simulations.

All biophysical simulations were run using the NEURON simulation environment (Hines and Carnevale (1997)). The model was implemented in Python using the PyNEURON interface (Hines *et al.* (2009)). The code for the model will be made available on the Assisi lab GitHub page (`https://github.com/assisilab`) at a suitable time.

3.1 Single-Cell Simulations

To test if we could replicated the changes in ISI observed in Marcantoni *et al.* (2014), we created a single-compartment model of a layer II stellate cell in the medial entorhinal cortex, and simulated the cell's behaviour in isolation for 1 second of activity; first without the presence of voltage-gated calcium channels and then with the channels present. These cells fire spontaneously, and thus needed no external input to generate action potentials. We recorded the membrane potential of the cell and calculated the average ISI of the spikes generated. The results of these experiments will be discussed in §4.1.

3.2 Network Simulations

These simulations were set up as described in §2.2.3. The network model of the entorhinal cortex was simulated for 30 seconds of activity, and the activity of the SC and IN rings was recorded.

3.2.1 Manipulations of calcium homeostasis timescales

As an important second messenger molecule, calcium plays a crucial role in various intracellular regulatory processes. Thus, healthy cells have multiple mechanisms to maintain calcium homeostasis, ensuring that calcium messaging is reliable and efficient. One of the most important organelles involved in calcium homeostasis is the endoplasmic reticulum (ER), which acts as a sequestering site for calcium ions and a regulator of intracellular calcium dynamics. It is also known that these homeostatic mechanisms break down in AD, and disrupted calcium signalling creates a cascade of detrimental cellular effects (Wang *et al.* (2017); Yu *et al.* (2009)).

To simulate the breakdown of the ER's ability to sequester calcium, we manipulated the timescale of the calcium dynamics in the model by changing the time constant of the calcium decay in the SCs. We ran the network model with the default "healthy" calcium decay timescale (τ_{Ca}), and altered this timescale in steps to model the reduced efficacy of the ER in sequestering calcium ions in AD.

3.2.2 Manipulations of Maximum Afterhyperpolarization Conductance

As discussed in §1.3.2, the electrophysiological properties of K_{Ca} channels in the entorhinal cortex are altered in AD, although the exact nature of these changes is still the subject of active research. More specifically, we have discussed studies that imply that the maximal conductances of K_{Ca} channels are altered in AD, leading to changes in the firing properties of the cells. While our AHP current model (described in §2.1.1) is a gross simplification of the complex biophysics of the multiple K_{Ca} channels present in EC SCs, we believe that for the purpose of an exploratory study this model is sufficient. To investigate the effects of these changes, we manipulated the maximal conductance ($\bar{g}_{K_{Ca}}$) of the afterhyperpolarization current (I_{AHP}) in the SCs. We ran simulations with the default $\bar{g}_{K_{Ca}}$ value of 0.01 S/cm^2, and reduced the conductance in steps to try and reflect the hyperexcitability of EC SCs in AD, as discussed in §1.3.2.

3.3 Mathematical Analysis

3.3.1 Decoding Spikes and Path Integration

We can decode the position of the simulated animal from the spiking data from SCs in the network model, using the following calculations. Each SC is

assigned a phase ϕ_k based of its index k in the network, which runs from 0 to $N-1$, where N is the number of SCs in a ring.

$$\phi_k = \frac{2\pi k}{N}$$

Then, we create a complex population vector $P(t)$, using the scalar firing rate of the SCs ($r_k(t)$) and the phase of each SC (ϕ_k).

$$P(t) = \sum_{k=1}^{N} r_k(t) e^{i\phi_k}$$

Here, $P(t)$ is the phase-weighted average of the firing rates of the SCs in the network. To get the decoded phase $\Phi(t)$ from $P(t)$, we can simply take the resultant angle of the weighted average.

$$\Phi(t) = \arg(P(t))$$

3.3.2 Circular Variance

To quantify the spread of the phase of the SCs in the network, we can run multiple simulations of the network model and record the decoded phases of the SCs at each time step. Let the decoded phase at time t from the j^{th} simulation be $\Phi_j(t)$. We can then calculate the circular variance, which is a measure of the spread of the decoded phases across the 100 simulations. The circular variance is defined as:

$$1 - \left| \frac{1}{n} \sum_{k=1}^{n} e^{i\Phi_j(t)} \right|$$

where n is the number of simulations. This function was implemented in Python using the SciPy library.

Chapter 4

Results

In this chapter, we shall discuss the most salient results obtained over the course of this project.

4.1 Spike Frequency Adaptation in Isolated SCs

As seen in the voltage traces in Figures 4.1a, 4.1b, and 4.1c, the stellate cell model exhibits spike frequency adaptation when both voltage-gated calcium channels (VGCC) and afterhyperpolarization (AHP) currents are present, but not when the AHP currents are missing. Moreover, the average interspike interval (ISI) of the stellate cell model under the effects of different calcium dynamics is shown in Figure 4.1d, and as we can see, the ISI is significantly increased from the control (no VGCC or AHP currents) simulation when both VGCC and AHP currents are present, but not with calcium dynamics alone. This implies that the K_{Ca} channels are largely responsible for the spike frequency adaptation, replicating the experimental results of Khawaja *et al.* (2007) who proved that K_{Ca} channels are responsible for spike frequency adaptation in EC stellate cells.

Applying the manipulations we described in §3.2.1 and §3.2.2, we can clearly see that it is possible to induce lower ISI in the isolated SC model by reducing the calcium decay timescale (τ_{Ca}) or reducing the maximal conductance of the afterhyperpolarization current ($\bar{g}_{K_{Ca}}$). This is shown in Figures 4.2a and 4.2b respectively. Thus, it is possible to alter the electrophysiological properties of the cell to reflect the reduced ISI observed in AD, as described by Marcantoni *et al.* (2014) (detailed in §1.3.2).

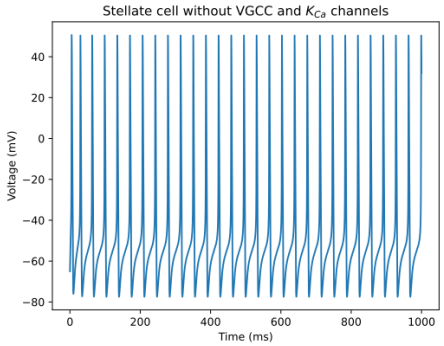

(a) No calcium dynamics

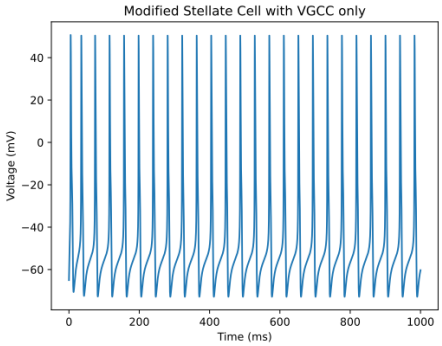

(b) Only VGCC currents

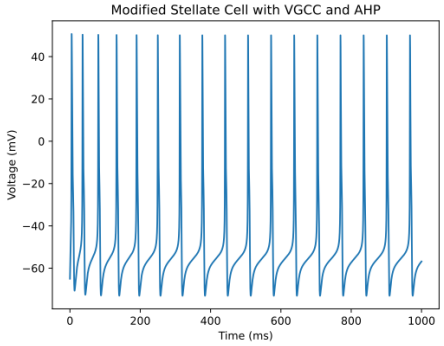

(c) VGCC and AHP

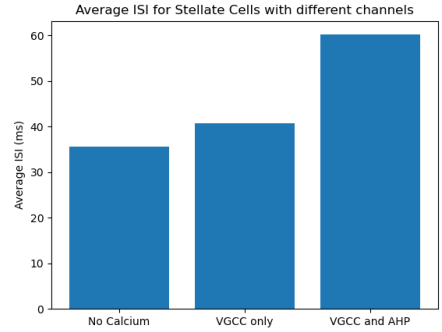

(d) ISI

Figure 4.1: Spike frequency adaptation in stellate cell models with different calcium dynamics, and average ISI in these different simulations. Note that the ISI is almost doubled when both VGCC and AHP currents are present in comparison to the other two conditions.

4.2 Network Behaviour

While the previous section gave us valuable insights into the behaviour of our SC model in isolation, we must also consider its behaviour in a network setting, and confirm that the manipulations discussed above have the desired effects when the network is taken as a whole rather than the sum of its parts.

First, we ran the network model with and without the the presence of I_{AHP} currents in the SCs, and recorded the spiking activity of the SC and IN rings. Comparing the raster plots in Figures 4.3a and 4.3b, we can see that the ISI clearly decreases when no I_{AHP} currents are present in the SCs, as expected from our single cell results. However, we also see that the bursting activity of the SCs is widened when I_{AHP} currents are present, which is

unexpected! Here, we see the SCs become more excitable (as described in Heggland *et al.* (2019)) when we change $\bar{g}_{K_{Ca}}$ in the opposite direction! This is a clear indication that the network behaviour is not a one-to-one replica of the behaviour of the isolated SC model. Moreover, it presents us with a dilemma: it seems that our model cannot produce both the reduced ISI and the widened bursting activity (indicative of increased excitability) in SCs at the same time.

Similarly, as shown in Figure 4.4, we see that the ISI decreases with decreasing τ_{Ca} in the network model, just like in the isolated SC model. However, the bursting is widened for the high τ_{Ca} case, which is again unexpected. These results imply that either the model is too simple to capture the full complexity of the changes occurring in AD that lead to the electrophysiological properties described in Heggland *et al.* (2019) and Marcantoni *et al.* (2014) simultaneously, or that the changes observed in one of these properties (reduced ISI or hyperexcitability) might be an experimental artifact: after all, the electrophysiological properties of the cells were measured in isolation and in response to injected currents in these studies, and as we have shown with our network model, the microcircuits in the can show emergent properties not captured by the studies mentioned above.

4.3 Errors in path integration

We calculated the path integration errors in the network model as described in §3.3.2 for network simulations over 30 seconds for different values of $\bar{g}_{K_{Ca}}$ and τ_{Ca}. As shown in Figure 4.5a, there are no significant changes in the path integration errors with changing $\bar{g}_{K_{Ca}}$. However, as shown in Figure 4.5b, the path integration errors reduce slightly with increased τ_{Ca}.

This is an interesting result, as it implies that the network model is more accurate in path when τ_{Ca} is higher. Here, we see that our network model is able to "deal" with increased excitability in the SCs caused by the accumulation of Ca^{2+} ions due to the increased calcium decay timescale. As seen in Figures 4.4 and 4.2a, simulations with lower τ_{Ca} have lower ISI, and these are the same simulations with greater path integration errors. Thus, our results agree with the experimental findings of Marcantoni *et al.* (2014), and suggest that the SC hyperexcitability observed in Heggland *et al.* (2019) is not the imperative cause of path integration defects in early stage AD, a conclusion supported by the fact that another study (Jun *et al.* (2020)) found no hyperexcitability in MEC SCs from APP-KI mice.

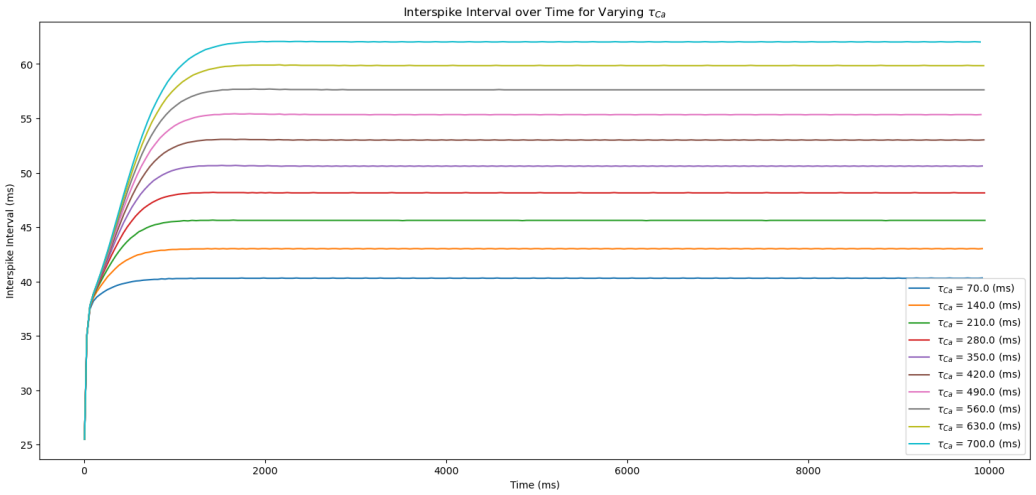

(a) ISI vs τ_{Ca}

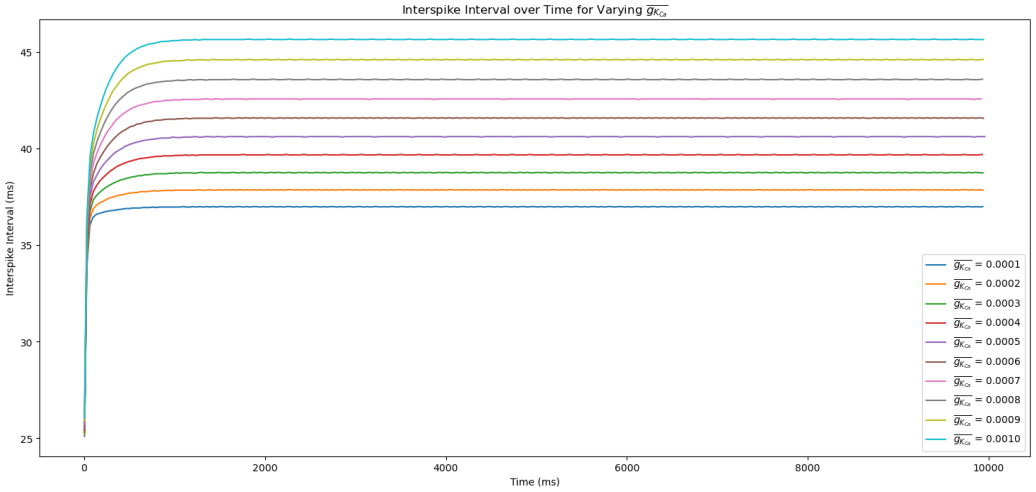

(b) ISI vs $\bar{g}_{K_{Ca}}$

Figure 4.2: These plots depict the time evolution of the ISI of the single stellate cell model with varying (a) calcium decay timescales and (b) maximal conductances of the afterhyperpolarization current.

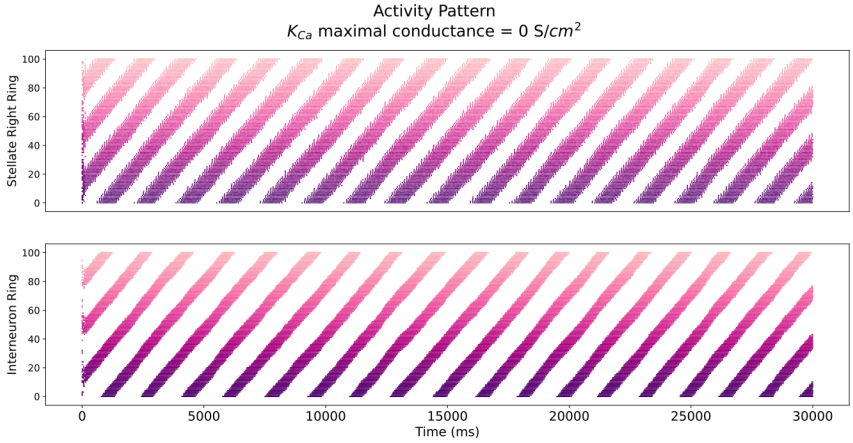

(a) No calcium dynamics

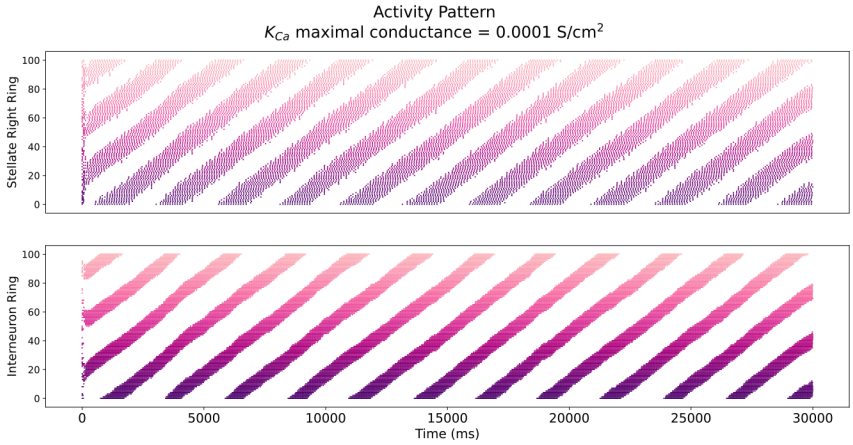

(b) With calcium dynamics

Figure 4.3: Raster plots of spikes in the active SC and IN rings the network model with (a) and without (b) calcium dynamics. Note the sparser yet widened bursting in SCs when calcium dynamics are present.

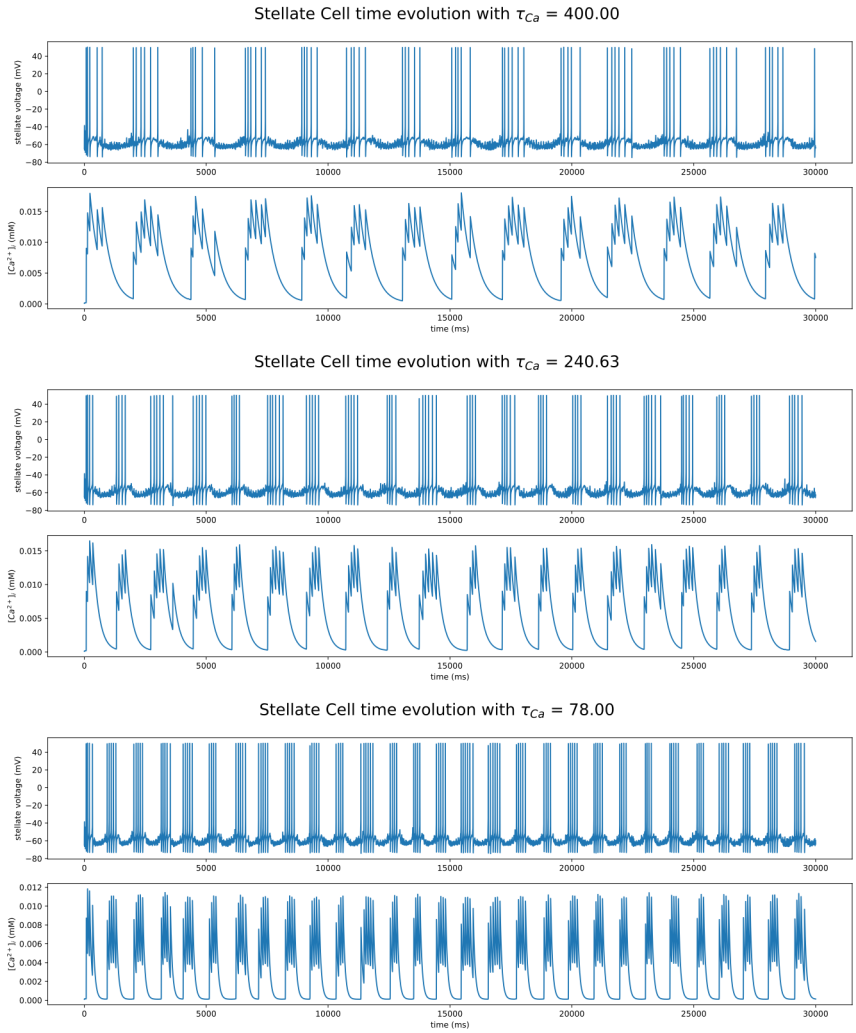

Figure 4.4: Effects of decreasing τ_{Ca} on the activity of an SC in the network model. The ISI decreases with decreasing τ_{Ca}, just like with an isolated SC

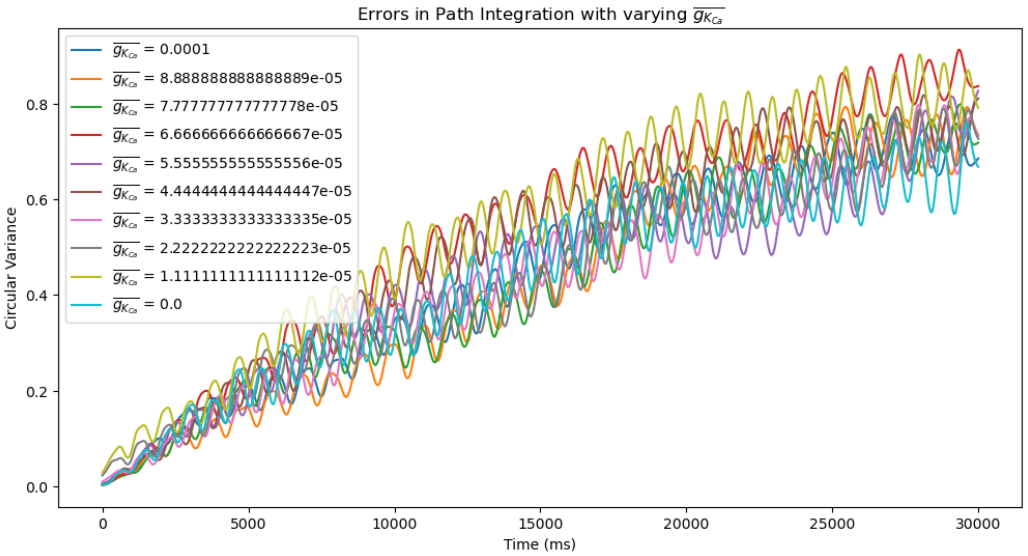

(a) Path integration errors with changing $\bar{g}_{K_{Ca}}$

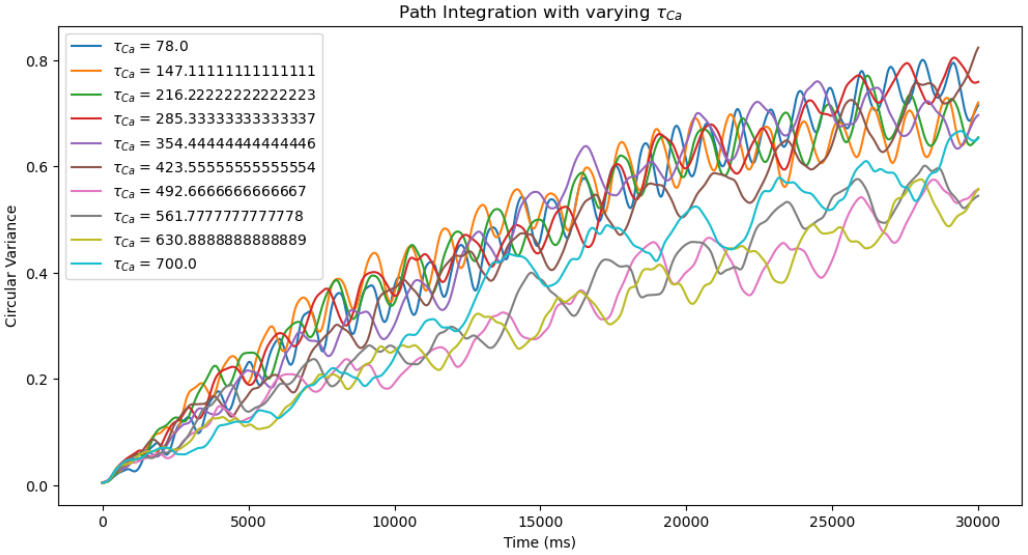

(b) Path integration errors with changing τ_{Ca}

Figure 4.5: Path integration errors in the network model. The errors are calculated as described in §3.3.2.

Chapter 5

Discussion

5.1 Concluding Remarks

The mechanisms that kick off the cellular cascades that cause the characteristic cellular damage in AD are still not well understood. Insights into the early stages of the disease are especially confounded, due to the fact that model transgenic lines are often engineered to express proteins like APP that overexpressed in AD, which may just be symptoms of a different "underlying cascade" in *in vivo* cases of AD. This is supported by the mountains of literature with often conflicting results on the electrophysiological effects of amyloid-β on cells.

While several other lines of research are indeed hunting for these proposed underlying cascades, we propose that understanding the effects of electrophysiological changes that occur in model animals in a network simulation could be a useful tool to filter through mechanisms that are not likely to be involved in the early stages of *in vivo* AD. For instance, if a proposed mechanism in a new AD model line creates changes that, upon simulation, do not result in the characteristic spatial integration deficits observed in AD, than it is likely that the given mechanism is not the "whole story".

Our report also showed that altered calcium homeostatic mechanisms had a more significant effect on the spatial integration performance of the network than the altered I_{AHP} conductance. This is interesting, as the I_{AHP} conductance is often cited as a major player in the electrophysiological changes that occur in AD. This suggests that either *in vivo* grid cell microcircuits may be able to compensate for changes in K_{Ca} channel properties in grid cells, or that our model not detailed enough to accurately represent the effects of altered electrophysiological properties of SC K_{Ca} channels on grid cell function in AD.

5.2 Future Directions

As mentioned above and in Chapter 2, our model, though biophysically realistic and tractable, is still a gross oversimplification of the sheer diversity of ionic and molecular mechanisms that are likely involved in the electrophysiological changes that occur in AD. For example, the model compresses all K_{Ca} conductances into a single I_{AHP} current, despite the overwhelming evidence that there are several different types of K_{Ca} channels in layer II SCs of the MEC. Moreover, we have also simplified the vast array of homeostatic mechanisms that are likely involved in the regulation of calcium into a single first-order differential equation. Simplifications like these are necessary to make simulating the model feasible, but also casts doubt over the veracity of this study's findings. While this level of detail is sufficient for an exploratory study, better insights would be gained by creating a more detailed model. Perhaps separating out different K_{Ca} conductances and explicitly modelling more realistic regulatory mechanisms like the Ryanodine receptors and the SERCA pumps, with an additional compartment to model the ER, would provide a more accurate representation of the intracellular dysfunction that occurs in AD.

References

Bateman RJ, Xiong C, Benzinger TLS, Fagan AM, Goate A, Fox NC, Marcus DS, Cairns NJ, Xie X, Blazey TM, Holtzman DM, Santacruz A, Buckles V, Oliver A, Moulder K, Aisen PS, Ghetti B, Klunk WE, McDade E, Martins RN, Masters CL, Mayeux R, Ringman JM, Rossor MN, Schofield PR, Sperling RA, Salloway S, Morris JC (2012). Clinical and Biomarker Changes in Dominantly Inherited Alzheimer's Disease. New England Journal of Medicine 367(9), 795–804.

Bazhenov M, Stopfer M, Rabinovich M, Huerta R, Abarbanel HDI, Sejnowski TJ, Laurent G (2001). Model of Transient Oscillatory Synchronization in the Locust Antennal Lobe. Neuron 30(2), 553–567.

Bellmund JLS, Gärdenfors P, Moser EI, Doeller CF (2018). Navigating cognition: Spatial codes for human thinking. Science 362(6415), eaat6766.

Bierbrauer A, Kunz L, Gomes CA, Luhmann M, Deuker L, Getzmann S, Wascher E, Gajewski PD, Hengstler JG, Fernandez-Alvarez M, Atienza M, Cammisuli DM, Bonatti F, Pruneti C, Percesepe A, Bellaali Y, Hanseeuw B, Strange BA, Cantero JL, Axmacher N (2020). Unmasking selective path integration deficits in Alzheimer's disease risk carriers. Science Advances 6(35), eaba1394.

Boudoulas KD, Triposkiadis F, Stefanadis C, Boudoulas H (2017). The endlessness evolution of medicine, continuous increase in life expectancy and constant role of the physician. Hellenic Journal of Cardiology 58(5), 322–330.

Breijyeh Z, Karaman R (2020). Comprehensive Review on Alzheimer's Disease: Causes and Treatment. Molecules 25(24), 5789.

Buchhave P, Minthon L, Zetterberg H, Wallin ÅK, Blennow K, Hansson O (2012). Cerebrospinal Fluid Levels ofβ-Amyloid 1-42, but Not of Tau, Are Fully Changed Already 5 to 10 Years Before the Onset of Alzheimer Dementia. Archives of General Psychiatry 69(1), 98–106.

Burgess N (2014). The 2014 Nobel Prize in Physiology or Medicine: A Spatial Model for Cognitive Neuroscience. Neuron 84(6), 1120–1125.

Burgess N, O'Keefe J (2011). Models of place and grid cell firing and theta rhythmicity. Current Opinion in Neurobiology 21(5), 734–744.

Chin J, Massaro CM, Palop JJ, Thwin MT, Yu GQ, Bien-Ly N, Bender A, Mucke L (2007). Reelin Depletion in the Entorhinal Cortex of Human Amyloid Precursor Protein Transgenic Mice and Humans with Alzheimer's Disease. J Neurosci 27(11), 2727–2733.

Couey JJ, Witoelar A, Zhang SJ, Zheng K, Ye J, Dunn B, Czajkowski R, Moser MB, Moser EI, Roudi Y, Witter MP (2013). Recurrent inhibitory circuitry as a mechanism for grid formation. Nat Neurosci 16(3), 318–324.

Cox D, Cui J, Aldrich R (1997). Allosteric Gating of a Large Conductance Ca-activated K+ Channel. J Gen Physiol 110(3), 257–281.

Cox DH (2014). Modeling a Ca2+ Channel/BKCa Channel Complex at the Single-Complex Level. Biophysical Journal 107(12), 2797–2814.

Dubois B, Hampel H, Feldman HH, Scheltens P, Aisen P, Andrieu S, Bakardjian H, Benali H, Bertram L, Blennow K, Broich K, Cavedo E, Crutch S, Dartigues JF, Duyckaerts C, Epelbaum S, Frisoni GB, Gauthier S, Genthon R, Gouw AA, Habert MO, Holtzman DM, Kivipelto M, Lista S, Molinuevo JL, O'Bryant SE, Rabinovici GD, Rowe C, Salloway S, Schneider LS, Sperling R, Teichmann M, Carrillo MC, Cummings J, Jack CR (2016). Preclinical Alzheimer's disease: Definition, natural history, and diagnostic criteria. Alzheimers Dement 12(3), 292–323.

Fagan AM, Xiong C, Jasielec MS, Bateman RJ, Goate AM, Benzinger TLS, Ghetti B, Martins RN, Masters CL, Mayeux R, Ringman JM, Rossor MN, Salloway S, Schofield PR, Sperling RA, Marcus D, Cairns NJ, Buckles VD, Ladenson JH, Morris JC, Holtzman DM, THE DOMINANTLY INHERITED ALZHEIMER NETWORK (2014). Longitudinal Change in CSF Biomarkers in Autosomal-Dominant Alzheimer's Disease. Science Translational Medicine 6(226), 226ra30–226ra30.

Funato H, Yoshimura M, Kusui K, Tamaoka A, Ishikawa K, Ohkoshi N, Namekata K, Okeda R, Ihara Y (1998). Quantitation of amyloid beta-protein (A beta) in the cortex during aging and in Alzheimer's disease. Am J Pathol 152(6), 1633–1640.

Galimberti D, Scarpini E (2011). Disease-modifying treatments for Alzheimer's disease. Ther Adv Neurol Disord 4(4), 203–216.

Giocomo LM, Moser MB, Moser EI (2011). Computational Models of Grid Cells. Neuron 71(4), 589–603.

Gómez-Isla T, Price JL, Jr DWM, Morris JC, Growdon JH, Hyman BT (1996). Profound Loss of Layer II Entorhinal Cortex Neurons Occurs in Very Mild Alzheimer's Disease. J Neurosci 16(14), 4491–4500.

Hafting T, Fyhn M, Molden S, Moser MB, Moser EI (2005). Microstructure of a spatial map in the entorhinal cortex. Nature 436(7052), 801–806.

Hardy JA, Higgins GA (1992). Alzheimer's Disease: The Amyloid Cascade Hypothesis. Science 256(5054), 184–185.

Heggland I, Kvello P, Witter MP (2019). Electrophysiological Characterization of Networks and Single Cells in the Hippocampal Region of a Transgenic Rat Model of Alzheimer's Disease. eNeuro 6(1).

Hines M, Davison AP, Muller E (2009). NEURON and Python. Front Neuroinform 3.

Hines ML, Carnevale NT (1997). The NEURON Simulation Environment. Neural Computation 9(6), 1179–1209.

Hodgkin AL, Huxley AF (1952). A quantitative description of membrane current and its application to conduction and excitation in nerve. J Physiol 117(4), 500–544.

Høydal ØA, Skytøen ER, Andersson SO, Moser MB, Moser EI (2019). Object-vector coding in the medial entorhinal cortex. Nature 568(7752), 400–404.

Igarashi KM (2023). Entorhinal cortex dysfunction in Alzheimer's disease. Trends in Neurosciences 46(2), 124–136.

Jun H, Bramian A, Soma S, Saito T, Saido TC, Igarashi KM (2020). Disrupted Place Cell Remapping and Impaired Grid Cells in a Knockin Model of Alzheimer's Disease. Neuron 107(6), 1095–1112.e6.

Khawaja FA, Alonso AA, Bourque CW (2007). Ca2+-dependent K+ currents and spike-frequency adaptation in medial entorhinal cortex layer II stellate cells. Hippocampus 17(12), 1143–1148.

Liu CC, Liu CC, Kanekiyo T, Xu H, Bu G (2013). Apolipoprotein E and Alzheimer disease: Risk, mechanisms and therapy. Nat Rev Neurol 9(2), 106–118.

Marcantoni A, Raymond EF, Carbone E, Marie H (2014). Firing properties of entorhinal cortex neurons and early alterations in an Alzheimer's disease transgenic model. Pflugers Arch - Eur J Physiol 466(7), 1437–1450.

Mittal D, Narayanan R (2018). Degeneracy in the robust expression of spectral selectivity, subthreshold oscillations, and intrinsic excitability of entorhinal stellate cells. Journal of Neurophysiology 120(2), 576–600.

Neru A, Assisi C (2021). Theta Oscillations Gate the Transmission of Reliable Sequences in the Medial Entorhinal Cortex. eNeuro 8(3), ENEURO.0059–20.2021.

Nilssen ES, Jacobsen B, Fjeld G, Nair RR, Blankvoort S, Kentros C, Witter MP (2018). Inhibitory Connectivity Dominates the Fan Cell Network in Layer II of Lateral Entorhinal Cortex. J Neurosci 38(45), 9712–9727.

O'Keefe J (1976). Place units in the hippocampus of the freely moving rat. Experimental Neurology 51(1), 78–109.

O'Keefe J, Burgess N (1996). Geometric determinants of the place fields of hippocampal neurons. Nature 381(6581), 425–428.

O'Keefe J, Dostrovsky J (1971). The hippocampus as a spatial map: Preliminary evidence from unit activity in the freely-moving rat. Brain Research 34, 171–175.

O'Keefe J, Nadel L (1978). The Hippocampus as a Cognitive Map. Clarendon Press.

Pérez-García CG, González-Delgado FJ, Suárez-Solá ML, Castro-Fuentes R, Martín-Trujillo JM, Ferres-Torres R, Meyer G (2001). Reelin-immunoreactive neurons in the adult vertebrate pallium. Journal of Chemical Neuroanatomy 21(1), 41–51.

Petersen RC, Smith GE, Waring SC, Ivnik RJ, Tangalos EG, Kokmen E (1999). Mild Cognitive Impairment: Clinical Characterization and Outcome. Archives of Neurology 56(3), 303–308.

Poirazi P, Brannon T, Mel BW (2003). Arithmetic of Subthreshold Synaptic Summation in a Model CA1 Pyramidal Cell. Neuron 37(6), 977–987.

Reitz C, Brayne C, Mayeux R (2011). Epidemiology of Alzheimer disease. Nat Rev Neurol 7(3), 137–152.

Schlesiger MI, Boublil BL, Hales JB, Leutgeb JK, Leutgeb S (2018). Hippocampal Global Remapping Can Occur without Input from the Medial Entorhinal Cortex. Cell Reports 22(12), 3152–3159.

Schöder H, Gönen M (2007). Screening for Cancer with PET and PET/CT: Potential and Limitations. Journal of Nuclear Medicine 48(1 suppl), 4S–18S.

Solstad T, Boccara CN, Kropff E, Moser MB, Moser EI (2008). Representation of Geometric Borders in the Entorhinal Cortex. Science 322(5909), 1865–1868.

Sperling RA, Jack CR, Aisen PS (2011). Testing the Right Target and the Right Drug at the Right Stage. Sci Transl Med 3(111), 111cm33.

Taube JS, Muller RU, Ranck JB (1990). Head-direction cells recorded from the postsubiculum in freely moving rats. I. Description and quantitative analysis. J Neurosci 10(2), 420–435.

Tolman EC (1948). Cognitive maps in rats and men. Psychological Review 55(4), 189–208.

Topczewska A, Evans T, Pratt W, Burgess N, Dolphin AC, Shah M (2019). T-Type Ca2+ Channels and Layer II Medial Entorhinal Cortical Stellate Cell Excitability. Biophysical Journal 116(3), 9a.

Trombetta-Lima M, Krabbendam IE, Dolga AM (2020). Calcium-activated potassium channels: Implications for aging and age-related neurodegeneration. The International Journal of Biochemistry & Cell Biology 123, 105748.

Wang L, Kang H, Li Y, Shui Y, Yamamoto R, Sugai T, Kato N (2015). Cognitive recovery by chronic activation of the large-conductance calcium-activated potassium channel in a mouse model of Alzheimer's disease. Neuropharmacology 92, 8–15.

Wang Y, Shi Y, Wei H (2017). Calcium Dysregulation in Alzheimer's Disease: A Target for New Drug Development. J Alzheimers Dis Parkinsonism 7(5), 374.

Yaari R, Fleisher AS, Tariot PN (2011). Updates to Diagnostic Guidelines for Alzheimer's Disease. Prim Care Companion CNS Disord 13(5), PCC.11f01262.

Yamamoto K, Ueta Y, Wang L, Yamamoto R, Inoue N, Inokuchi K, Aiba A, Yonekura H, Kato N (2011). Suppression of a Neocortical Potassium Channel Activity by Intracellular Amyloid-β and Its Rescue with Homer1a. J Neurosci 31(31), 11100–11109.

Yokoyama M, Kobayashi H, Tatsumi L, Tomita T (2022). Mouse Models of Alzheimer's Disease. Front Mol Neurosci 15, 912995.

Yu JT, Chang RCC, Tan L (2009). Calcium dysregulation in Alzheimer's disease: From mechanisms to therapeutic opportunities. Progress in Neurobiology 89(3), 240–255.